Predicting Relative Binding Free Energies of Tacrine−Huperzine A Hybrids as Inhibitors of Acetylcholinesterase[§]

Xavier Barril,[†] Modesto Orozco,*[,‡] and F. Javier Luque*[,†]

Departament de Fisicoquímica, Facultat de Farmàcia, Universitat de Barcelona, Avgda. Diagonal 643, 08028 Barcelona, Spain, and Departament de Bioquímica i Biologia Molecular, Facultat de Química, Universitat de Barcelona, Martí i Franqués 1, 08028 Barcelona, Spain

Received July 19, 1999

The binding of the 9-methyl derivative of tacrine−huperzine A hybrid to *Torpedo californica* acetylcholinesterase (AChE) has been studied by computational methods. Molecular dynamics simulations have been performed for the AChE−drug complex considering two different ionization states of the protein and two different orientations of the drug in the binding pocket, which were chosen from a previous screening procedure. Analysis of structural fluctuations and of the pattern of interactions between drug and enzyme clearly favor one binding mode for the tacrine−huperzine A hydrid, which mixes effectively some of the binding features of tacrine and huperzine A. The differences in inhibitory activity for a series of related derivatives have been successfully predicted by free energy calculations, which reinforces the confidence in the binding mode and its usefulness for molecular modeling studies. The same techniques have been used to make de novo predictions for a new 3-fluoro-9-ethyl derivative, which can be used to verify a posteriori the goodness of the binding mode. Finally, we have also investigated the effect of replacing Phe300 in the *Torpedo californica* enzyme by Tyr, which is present in the human AChE. The results indicate that the Phe330→Tyr mutation is expected to have little effect on the binding affinities. Overall, the whole of results supports the validity of the putative binding model to explain the binding of tacrine−huperzine A hybrids to AChE.

Introduction

Alzheimer disease (AD)[32] is a neurodegenerative process associated with deposition of amyloid plaques and fibrillary tangles, as well as with neurotransmission damage in the brain.[1] One of the main functional deficits in AD involves cholinergic neurons, and this evidence provided the rational for a potential therapeutic approach to the treatment of AD.[2] Several strategies have been explored to enhance cholinergic transmission, such as acetylcholinesterase (AChE) inhibitors, acetylcholine precursors, muscarinic agonists, or acetylcholine releasers. To date AChE inhibition has proved to be the most successful strategy to ameliorate cholinergic deficit and to promote symptomatic improvement. Tacrine (THA; Figure 1) was the first inhibitor approved for the palliative treatment of AD senile dementia.[3] Its clinical efficacy, nevertheless, is limited owing to undesirable side effects, specially hepatotoxicity, and current research is focused on developing new inhibitors with improved activity and reduced adverse side effects.[4] Efforts have concentrated on analogues of tacrine,[5] as well as derivatives of physostigmine,[6] *N*-benzylpiperidines,[7] and xanthones.[8] Attention has also been paid to huperzine A (HUP; see Figure 1), an alkaloid found in *Huperzia serrata* traditionally utilized in Chinese folk medicine.[9]

Recently, a new compound named tacrine−huperzine A hybrid (HTH; see Figure 1) that mixes the 4-amino-quinoline ring system of THA with the carbobicyclic moiety of HUP has been synthesized and tested for AChE inhibition.[10] The (−)-enantiomer of the parent compound, 12-amino-6,7,10,11-tetrahydro-9-methyl-7,11-methanocycloocta[*b*]quinoline (9M-HTH; Figure 1), was around 3 times more active than THA in inhibiting AChE from bovine erythrocytes. The inhibitory potency was improved by replacing the methyl group at position 9 by an ethyl group and more markedly upon attachment of a fluoro subtituent to position 3, this latter compound being 40 times more active than THA in bovine erythrocyte AChE inhibitory assays,[11] which makes it very interesting for subsequent structure−activity studies.

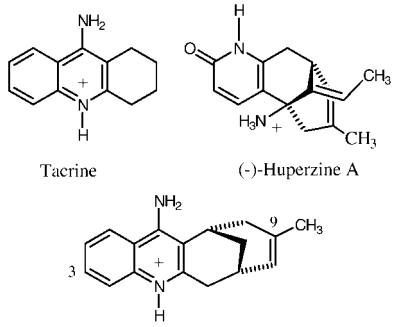

Figure 1. Schematic representation of the AChE inhibitors tacrine, (−)-huperzine A and the (−)-enantiomer of the tacrine−huperzine A hybrid.

Crystallographic structures for the AChE enzyme complexed with various inhibitors are available.[12−14] On the basis of the structures of AChE complexed with THA

* Address correspondence to these authors.
† Departament de Fisicoquímica.
‡ Departament de Bioquímica i Biologia Molecular.
§ Contribution from the Grup Especial de Recerca en Química Teòrica.

10.1021/jm990371u CCC: $18.00
Published on Web 11/25/1999

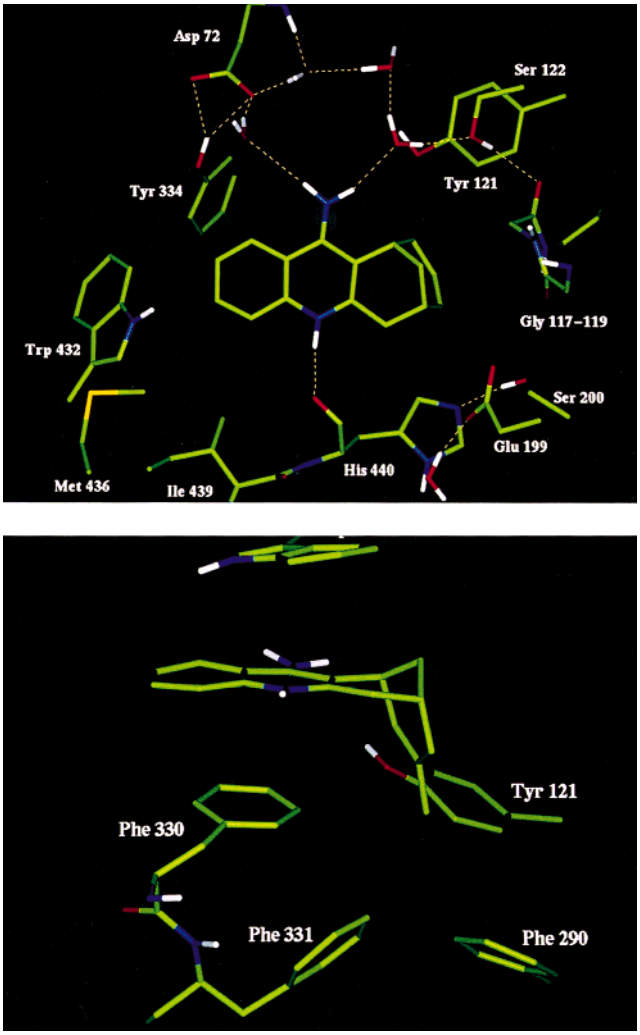

Figure 2. Plots of the main interactions between AChE and the (−)-enantiomer of the 9-methyl derivative of the tacrine−huperzine A hybrid positioned in the putative binding mode.

and HUP,[12,14,15] and after a wide screening of different orientations of the drug in the active site, we developed[11] a first binding model of tacrine−huperzine A hybrids to AChE. In the proposed model there exist a number of common structural features between the binding of the hybrid and the interactions observed in the crystallographic structures of THA and HUP complexed to AChE. Thus, the hybrid is stacked between the rings of Trp84 and Phe330 (Figure 2), as found for the AChE−THA complex. The NH_2 group occupies a position similar to that of the NH_2 in THA and the NH_3^+ in HUP when complexed to AChE. Indeed, the NH_2 group is well hydrated, and the water molecules link it directly or through water-mediated bridges to different residues such as Asp72 and Ser122. The NH group is hydrogen-bonded to the carbonyl oxygen of His440, which mimics a similar interaction found in the THA−AChE complex. Finally, the bicyclo[3.3.1]nonadiene subunit of the (−)-enantiomer occupies roughly the same position of the corresponding subunit of (−)-HUP in the AChE−HUP complex.

In this study we have refined the proposed binding mode through extended MD simulations. The reliability of the refined mode and its advantages with respect to alternative modes have been analyzed, and the key interactions responsible for the stability of the drug−protein complex have been determined. Knowledge of this information is essential to pursue our current studies for designing new chemical modifications leading to inhibitors with enhanced AChE affinity. To this end, we have performed molecular dynamics (MD) simulations to investigate the stability of the AChE−hybrid complex and to examine the occurrence of local structural changes in the residues forming the active site. These studies have been supplemented with free energy calculations carried out to predict differences in binding affinities for selected hybrid derivatives. Comparison of the relative binding free energies with the measured changes in inhibitory activity is valuable to further check the proposed binding model and to discuss the nature of the interactions that contribute to the binding. Finally, since calculations have been performed using the *Torpedo californica* enzyme structure, while the enzyme of interest is the human one, we have examined the effect of replacing Phe330 by Tyr on the binding of the hybrid inhibitors.

Methods

Setup of the Model. The simulation system was based on the crystal structure of the complex between *Torpedo californica* AChE and (−)-huperzine A.[14,15] The missing atoms from the original Protein Data Bank[16] file were built up using the program Insight-II.[17] The enzyme was modeled in its physiologically active form with neutral His440 and deprotonated Glu327, which form together with Ser200 the catalytic triad. The standard ionization state at neutral pH was considered for the rest of ionizable residues with the exception of Asp 392 and Glu443, which were neutral, and His471, which was protonated, according to previous numerical titration studies.[18] The geometry of the hybrid was fully optimized at the Hartree−Fock level with the 6-31G(d)[19] basis set using the Gaussian-94 program.[20] According to the basicity of the aminoquinoline ring,[21] the protonated species of the hybrid was considered in calculations. The hybrid was positioned in the crystallographic structure of the enzyme to fit the set of interactions involved in the proposed binding model[11] (Figure 2). The system was hydrated by centering a sphere of 25 Å of TIP3P[22] water molecules at the inhibitor. Particular attention was paid to filling the position of crystallographic waters inside and around the active site with TIP3P water molecules owing to their relevant structural role in AChE complexes with THA and HUP.[13,14] Those water molecules whose oxygen (hydrogen) atoms were less than 2.2 (1.8) Å from any residues of the protein were removed. The final model system (the protein, the inhibitor, and 670 TIP3P water molecules) was partitioned into a mobile region and a rigid region. The former included the inhibitor, all the protein residues containing at least one atom within 14 Å from the inhibitor, and all the water molecules, while the rest of atoms defined the rigid part. Both the mobile and the rigid regions were allowed to relax during the equilibration of the system, but only the mobile region was free to move in MD simulations.

Molecular Dynamics Simulations. Three different MD simulations were performed to examine the structural stability of the AChE complex with the 9-methyl derivative of the tacrine−huperzine A hybrid. The first simulation (A) explored the dynamics of the complex defined as mentioned above, i.e., with the enzyme in their catalytically active form and the drug positioned following the proposed binding mode (Figure 2). In the second simulation (B) we placed the inhibitor in a different orientation roughly related to the preceding one by a 180° rotation of the drug around the axis passing through the two nitrogen atoms. Finally, in a third simulation (C) the AChE−drug complex was built up using a different form of the enzyme, which is characterized by having protonated His440

and ionized Glu433 (see below for details about the choice of the alternative model systems).

In all cases the system was energy minimized in a sequential way. First, all hydrogen atoms were minimized for 1000 steps of steepest descent. Next, the position of water molecules was relaxed for 5000 steps of steepest descent. Finally, the whole system, including both mobile and rigid parts, was energy minimized for 2000 steps of steepest descent plus 3000 steps of conjugate gradients. At this point, we kept frozen the rigid part of the system and started the dynamic equilibration of the mobile part. This was accomplished in a series of four 10 ps MD simulations performed to increase the temperature of the mobile part up to 298 K. Subsequently, a 2 ns MD simulation was carried out for the different AChE−inhibitor complexes.

The AMBER-95 all-atom force-field[23] was used for the entire system except the hybrid compound. The charge distribution of the drug was determined from fitting to the HF/6-31G(d) electrostatic potential using the RESP[24] procedure, and the van der Waals parameters were taken from those defined for related atoms in the force field. SHAKE[25] was used to maintain all the bonds at their equilibrium distances, which allowed use of an integration time step of 2 fs. A cutoff of 11 Å was used for nonbonded interactions. The trajectory was stored every 1 ps for subsequent analysis of complexes. MD simulations were performed using the AMBER5 computer program.[26]

The relative stability of the AChE−drug complexes in simulations A, B, and C was examined from the average energy of the system determined using an approach[27] that combines the "gas phase" energy and the free energy of solvation computed with a continuum model. The analysis included 300 structures (100 for each simulation) taken during the last 0.5 ns of the simulations. For each solute configuration, the "gas phase" energy was computed from the AMBER-95 all-atom force field with no cutoff for nonbonded interactions. In these calculations all water molecules were ignored with the exception of a small subset located in the binding site, which were explicitly treated owing to their relevant structural role (see below). Free energies of solvation were reintroduced by using a Poisson−Boltzmann calculation for the electrostatic component and a surface-area-dependent term for the nonelectrostatic contribution. In Poisson−Boltzmann calculations the dielectric boundary was defined using a 1.4 Å probe sphere and atomic van der Waals radii taken from the AMBER-95 force field, which was also used to assign atomic charges. The solute was assigned a dielectric of 1, in agreement with the use of a nonpolarizable force field, and the solvent dielectric was set to 78.4. A cubic lattice (grid spacing of 0.35 Å) encompassing the complex (about 75% of the grid was occupied by the solute) was used in calculations, which were performed using 500 finite difference iterations (test calculations carried out with a larger number of iterations did not change significantly the computed free energy of solvation). These computations were performed with the program Delphi as implemented in Insight-II. The nonelectrostatic term was determined using a surface tension for all the atoms equal to 5.4 cal $Å^{-2}$.[28] No attempt was made to evaluate the solute entropy contribution, since this term is expected to be similar in the different simulations.

Free Energy Calculations. Thermodynamic integration (TI) calculations were performed with a 2-fold purpose. First, we investigated the effect of the changes hydrogen → fluorine at position 3 and methyl → ethyl at position 9 on the binding free energy of the parent compound. These simulations helped us to verify the reliability of the proposed binding mode, to understand the nature of the key drug−protein interactions, and to predict the inihibitory potency of a new drug. Second, we examined the effect of mutating the residue Phe330 in the *Torpedo californica* enzyme to Tyr residue, which is the corresponding residue in human AChE, on the binding affinities of the hybrid compounds. Such a mutation is the only relevant difference concerning the residues directly involved in the binding pocket between *Torpedo californica* and human enzymes. This simulation allows us to determine which changes can be expected in the results of the simulations due to the use of the protein structure of a different organism.

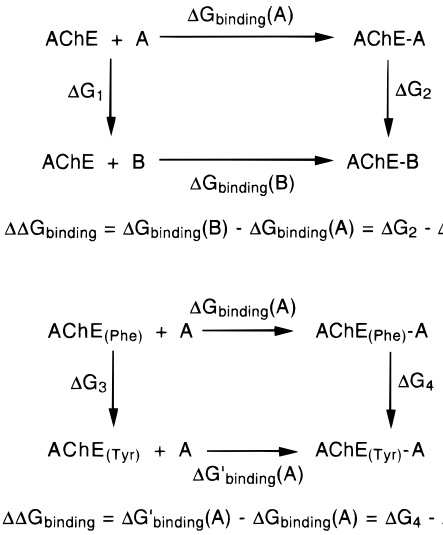

Figure 3. Thermodynamic cycles utilized in free-energy calculations to determine relative binding affinities between the inhibitors (top) and the influence of the mutation Phe330→Tyr on the free energy of binding (bottom).

The prediction of the relative binding free energies between inhibitors was based on the thermodynamic cycle shown in Figure 3 (top), where ΔG_1 and ΔG_2 denote the changes in free energy for mutating A to B in solution and in the AChE complex. Likewise, the influence of the Phe330→Tyr mutation on the drug binding was examined from the thermodynamic cycle shown in Figure 3 (bottom), where ΔG_3 and ΔG_4 stand for the free energy change corresponding to mutating those residues in the free enzyme and in the AChE−drug complex. The values of the different ΔG_i ($i = 1-4$) terms were determined using MD-TI calculations, which were carried out following the standard algorithm implemented in AMBER-5. Nonbonded intramolecular contributions were included in evaluating free energy differences.[29] The mutation between inhibitors in water and in the enzyme was performed using 41 windows, each window consisting of 5 ps for equilibration and 5 ps for averaging, leading to a total of 410 ps for each simulation. Test calculations performed using a 820 ps simulation predicted no relevant differences in the computed relative binding affinities due to the use of larger trajectories. All other technical details of MD-TI calculations are identical with those of MD simulations noted above.

To analyze the structural and energetic features of the interaction between the different drugs and the enzyme in the complexes formed with either the *Torpedo californica* enzyme or the mutated AChE, a series of 1.5 ns MD simulations were performed using the same technical features already noted.

Results and Discussion

Molecular Dynamics Simulations. In this section we examine the structural features of the complex between AChE in its physiological active form and the tacrine−huperzine A hybrid methylated at position 9 (9M-HTH), which was positioned in the binding pocket following the putative binding mode (Figure 2). The stability of the complex and the role of interactions with specific residues of the binding site are explored from the results of MD simulation of the AChE−drug complex (simulation A).

Further insight into the suitability of the binding model is gained by comparison with the results determined for two other simulations, where either the positioning of the drug (simulation B) or the ionization

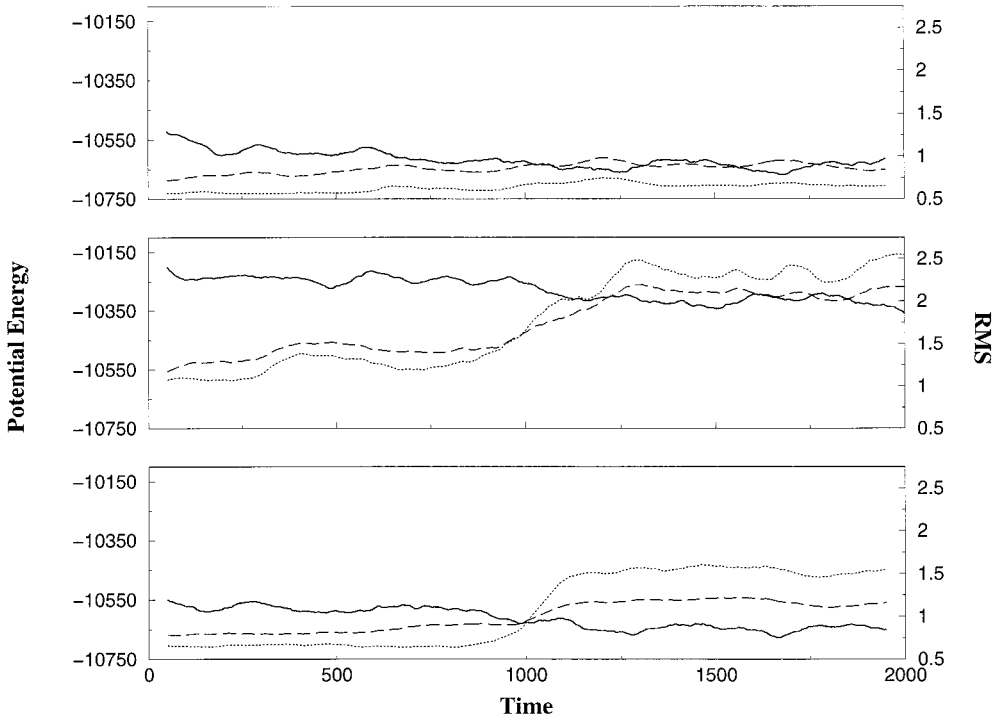

Figure 4. Time dependence of the potential energy (kcal/mol; solid line) and the RMS deviation (Å) for the AChE−drug system in simulations A (top), B (middle), and C (bottom). The rms deviation profiles are determined for all the heavy atoms in the mobile part (dashed line) and in the subset of residues (dotted line) forming the walls of the binding pocket. The profiles were smoothed in 100 ps windows for the sake of clarity.

state of the enzyme (simulation C) has been changed. In simulation B the inhibitor was placed in a different orientation which was not the most favored according to our previous screening studies.[11] This orientation roughly relates to the preceding one by a 180° rotation of the drug around the axis passing through the two nitrogen atoms. This rotation keeps unaltered most of the interactions concerning stacking of the quinoline ring system and contacts of the =N−H and $-NH_2$ groups, and mainly affects the position of the bicyclo subunit, which is surrounded by Gly80, Phe78, Met83, and Trp432. In simulation C the enzyme is considered in an alternative ionic state where His440 is protonated, while Glu443 is in its anionic form. Choice of this ionization state (where the enzyme is inactive) obeys previous numerical titration studies for the AChE−THA complex,[18] which indicated that this form of the complex is energetically close to the complex with the active form of the enzyme. This would make possible the involvement of an inhibition mechanism where the drug is trapped by an inactive form of the enzyme.

Simulation A. The AChE−drug system seems reasonably well equilibrated in the final part of the trajectory. The potential energy drops smoothly during the first 1 ns, but it remains nearly constant for the rest of the simulation (Figure 4). To examine the magnitude of the structural fluctuations occurring along the simulation, we computed the root-mean-square deviation (rmsd) from the X-ray structure of the enzyme for all the heavy atoms in the mobile region and in the subset of residues forming the walls of the binding site. The two rms profiles (see Figure 4) show a small increase of around 0.1 Å in the first 1 ns, and they remain stable for the rest of the simulation at values of 0.8 and 0.6 $Å^2$. The lack of relevant structural fluctuations both in the mobile region and in the neighborhood of the binding site evidences the stability of the drug−enzyme complex.

Analysis of the collected structures allowed us to determine key drug−protein interactions. Thus, the stacking of the drug between the rings of Trp84 and Phe330 seems essential for the binding, since it is fully maintained during all the simulation. The separation of the quinoline ring system from the indole and benzene rings amounts to 4.0 ± 0.5 and 3.9 ± 0.5 Å, respectively. The rings are roughly parallel, as noted in the angles formed between the planes of the quinoline subunit and of the indole or benzene rings, which are on average around 12°. The hydrogen bond between the N−H group and the carbonyl oxygen of His440 is also fully conserved (average N···O distance: 2.9 ± 0.1 Å). The NH_2 group is surrounded, on average, by two water molecules lying within 3.0−3.5 Å. One of these water molecules bridges the $-NH_2$ group to the carboxylate group of Asp72, and the other links the $-NH_2$ group mainly to the hydroxyl group of Ser122, and less frequently to that of Tyr121. All these water-mediated contacts are maintained along the simulation with the only exception of the water bridge with Asp72, whose side chain reorients during 200 ps after the first 1 ns leading to a transient loss of the water-mediated contact. After that period, the bridge with the $-NH_2$ group is recovered and remains until the end of the trajectory. Overall, this analysis indicates that the interactions between inhibitor and enzyme are well preserved along the simulation.

The time evolution of the interaction energy between 9M-HTH and the enzyme, as well as their electrostatic and van der Waals components, reveals no large fluctuations along the 2 ns simulation (data not shown). The interaction energy for the last 500 ps is, on average, −194.3 ± 9.1 kcal/mol. Analysis of the pairwise interac-

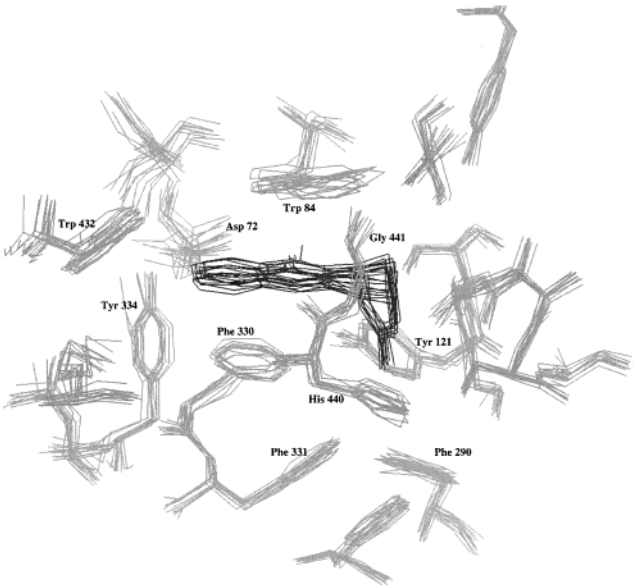

Figure 5. Superposition of the complex between the inhibitor 9M-HTH and the subset of residues forming the binding pocket for 10 structures collected every 50 ps during the last 0.5 ns of the simulation A.

tions between drug and residues in the binding pocket indicates relevant contributions for Asp72 (−47.0 ± 3.9 kcal/mol), Trp84 (−10.8 ± 1.3 kcal/mol), Phe330 (−5.4 ± 0.9 kcal/mol), His440 (−17.3 ± 1.1 kcal/mol), Glu199 (−51.4 ± 1.7 kca/mol), and Glu327 (−34.6 ± 0.7 kcal/mol). Overall, the preceding structural and energetic information indicates that the hybrid is firmly bound to the active site without suffering notable changes in the interactions with residues contributing to the binding, as can be stated from inspection of Figure 5, which superimposes 10 snapshots collected every 50 ps during the last 0.5 ns.

Simulation B. In this simulation the drug was positioned in a different orientation within the binding pocket of the enzyme, which was chosen following our preliminary studies (see above). The potential energy drops without abrupt changes until 1.2 ns, and then seems to be stable until the end of the simulation (Figure 4). The rmsd profiles for the heavy atoms in both the mobile part and the subset of residues forming the wall of the binding pocket show a continuous increase (Figure 5), reaching a value larger than 2 Å at the end of the simulation. This evidences the occurrence of relevant structural changes in the binding pocket, which are due to a drug reorientation along the simulation. In this process the drug remains stacked with the rings of Trp84 and Phe330 (average distances 4.2 ± 0.5 and 3.9 ± 0.5 Å; angle between ring planes 9.2° ± 5.0° and 18.5° ± 8.0°, respectively). Nevertheless, the bicyclo-[3.3.1]nonadiene unit pushes away a large number of residues, particularly Phe75, Phe78, Gly80, Ser81, Trp432, and Tyr442. Indeed, there are notable differences in the pattern of interactions mentioned above for simulation A. Thus, the hydrogen bond with the carbonyl group of His440 is lost (average N···O distance 4.6 ± 0.9 Å), and the water-mediated contacts of the $-NH_2$ group are remarkably more labile or even lost. For instance, the separation of the $-NH_2$ group and the Asp72 carboxylate oxygens varies from 3.5 to 6.5 Å. These structural changes are reflected in the interaction energy between drug and enzyme (average value −174.4 ± 17.6 kcal/mol), which is around 20 kcal/mol higher than that obtained in simulation A, and in the total potential energy of the simulated system (see Figure 4), which is around 300 kcal/mol higher than that of simulation A.

The structural and energetic instability of the binding mode explored in this simulation is in marked contrast with the results obtained in simulation A, where the rmsd remained unaltered at a significantly smaller value (around 0.7 Å) and all the interactions with residues in the binding pocket were well preserved along the simulation.

Simulation C. In this section we analyze the AChE−drug complex considering a different ionization state for the enzyme, which has protonated His440 and ionized Glu443 (see above). After thermalization the system seems to be equilibrated and the potential energy becomes stabilized after 1.2 ns (Figure 5). The rms deviation the heavy atoms in the mobile part increased around 0.3 Å along the simulation (Figure 5), which suggests that the global structure of the mobile region remains mostly unaltered. The rmsd profile for the residues forming the binding pocket increases near 1 Å at around 1 ns (Figure 5). Inspection of the structures collected before and after 1 ns shows two different effects contributing to this local structural rearrangement. First, the drug is moved away from the His440 owing to unfavorable electrostatic repulsion (see below; in fact, the =N−H···O=C= hydrogen bond is lost during the thermalization process), and such a displacement is transmitted to vicinal residues such as Trp84. Second, the contact observed in the crystallographic structure and in simulation A between Tyr334 and Asp72 is lost owing to the displacement of the inhibitor. In addition, the side chain of Tyr334 reorients and becomes exposed to the solvent.

The separation of the quinoline ring system from the indole and benzene rings of Trp84 and Phe330 is on average 3.8 ± 0.5 and 4.5 ± 0.5 Å. The planes of the quinoline and indole rings remain roughly parallel (the average angle between the rings is 10.5° ± 4.9°), but the angle formed with the benzene ring is 26.5° ± 10.9°, and values of around 60° are eventually reached. Thus, there is a weakening of the interaction with Phe330. The $-NH_2$ group is hydrated on average by two water molecules lying at 3.0−3.5 Å. One of them forms a bridge with the Asp72 carboxylate group, and the other interacts mainly with Tyr121. These contacts are, however, weaker than those found in simulation A. For instance, the separation of the amino nitrogen from the carboxylate oxygens increases from 5.0 ± 0.6 (Oδ1) and 6.2 ± 0.7 (Oδ2) Å in simulation A to 6.9 ± 1.0 and 6.6 ± 1.0 Å, respectively, in this simulation.

The preceding analysis points out notable structural fluctuations in the contacts of the drug with the residues forming the binding site. The average interaction energy (−184.0 ± 13.1 kcal/mol) between drug and enzyme is 10 kcal/mol higher than for simulation A. Looking at the contributions from specific residues, such a destabilization is motivated by the unfavorable electrostatic contact with the protonated His440 (+33.9 ± 1.7 kcal/mol), and the weakening of the interaction with Asp72

Table 1. Average Energies (kcal/mol) Determined for the AChE−Drug Complex in the Three Simulations[a]

energy[b]	A	B	C
"gas phase"			
bonded	4795.0 (17.3)	4828.5 (24.9)	4798.1 (17.5)
electrostatic	−17936.2 (27.4)	−18204.3 (38.0)	−17887.3 (29.2)
van der Waals	−2911.0 (19.7)	−2849.9 (17.0)	−2886.3 (16.5)
$\Delta E_{\text{gas phase}}$	0.0	−173.5	76.6
solvation			
Poisson−Boltzmann	−5329.5 (22.6)	−5098.0 (35.1)	−5395.3 (22.3)
nonpolar	98.7 (0.2)	98.8 (0.4)	99.6 (0.3)
$\Delta G_{\text{solvation}}$	0.0	231.6	−64.9
total	0.0	58.1	11.7

[a] Computed by averaging over 100 structures collected during the last 0.5 ns of the simulation. Standard deviations are in parentheses. [b] Relative values are given for the "gas phase", solvation, and total (gas phase + solvation) energies.

(−39.3 ± 3.4 kcal/mol) compared to the value obtained for simulation A.

Relative Stability of the AChE−Drug Complexes. The structural and energetic analysis of the three simulations noted above shows that the hydrid binds more firmly to AChE in its catalytically active form (simulation A) than in the other two cases. In simulation B the steric hindrance between the bicyclo-[3.3.1]nonadiene unit and the neighboring residues of the enzyme induces large structural rearrangements and a weakening in the drug binding. On the other hand, the electrostatic repulsion is the source of the structural distortion of the AChE−drug complex in simulation C. Since this form of the enzyme is catalytically ineffective, its involvement in the binding of the hybrid can be reasonably excluded.

To further examine the suitability of the binding model explored in simulation A, we determined the ensemble average ("gas phase" plus solvation) energies of the AChE−drug complexes in the three simulations. The results in Table 1 show that the complex in simulation A is clearly more stable than in simulation B. As expected from the large structural distortion originated by changing the drug orientation in the binding site (simulation B), both bonded and van der Waals energy contributions are destabilizing compared to the results in simulation A, but this effect is counterbalanced by favorable electrostatic contacts. Nevertheless, this latter contribution does not suffice to compensate the large destabilization due to solvation effects, leading to a net destabilization relative to simulation A. Inspection of sampled structures reveals the marked structural distortion of the backbbone, which reduces the hydration of the protein. This finding supports our previous results,[11] which suggested that the binding mode in simulation B was unable to explain the relative activity for a series of hybrid derivatives.

The results (see Table 1) also show that electrostatics and solvation are the most sensitive contributions in simulation C. Comparison of the relative stability between simulations A and C cannot be directly gained from the results in Table 1 owing to the change in internal energy of these residues upon ionization. To estimate the relative stability between the AChE−drug complexes in simulations A and C, we have combined the results in Table 1 with the free energy difference between neutral and ionized His and Glu at neutral pH and the cost of transferring the neutral (ionized) residues from the protein (water) to water (protein).[30] The first term was estimated from the experimental pK_a's of the residues in water, and the two remaining contributions were computed from Poisson−Boltzmann calculations. As a result, the AChE−drug complex in simulation C is found to be destabilized by nearly 40 kcal/mol relative to the complex in simulation A.

Overall, despite numerical uncertainties, the structural and energetic analysis of the sample structures collected in the simulations supports the suitability of the binding mode of the hybrid compounds to AChE considered in simulation A (see Figure 2), which will be used to predict the relative binding affinities of selected hybrid derivatives and compare them with the available experimental inhibitory data.

Relative Binding Affinities. Calculations were performed for the mutations hydrogen → fluorine at position 3 and methyl → ethyl at position 9 of the 9M-HTH compound. These substitutions involve contacts of the drug with the binding pocket in two distant regions and they lead to well-defined changes in the binding affinity for the series of hybrid compounds tested for AChE inhibition.[11] Thus, attachment of a fluorine atom at position 3 of (−)-9M-HTH increased ∼15-fold the inhibitory activity, and the IC_{50} of (−)-9M-HTH decreased by a factor of ∼2 upon replacement of methyl by ethyl. Finally, we also examined the effect of introducing simultaneously the two mutations in the parent compound to verify the additivity of the changes on the predicted binding affinities. There is no experimental information on the activity of this compound, and this could be used as a test of the binding model in future studies.

Comparison of selected structural and energetic properties for the complexes between *Torpedo californica* AChE and the hybrid derivatives is shown in Table 2. These properties were determined by averaging the corresponding values for the structures collected in the last 0.5 ns of a series of 1.5 ns MD simulations for the different AChE−drug complexes. The results reveal the lack of significant structural alterations, and the drug−enzyme interaction pattern is maintained in all cases. In fact, for most properties the differences observed between the average values are similar to or lower than the corresponding standard deviation of the measured property. Either attachment of fluorine or extension from methyl to ethyl leads to larger rms deviations relative to 9M-HTH. However, when the two modifications are made simultaneously, the rmsd values decrease and compare with those of 9M-HTH. This suggests a sort of balance between the effects arising from the two substitutions, which tend to reinforce the fitting of the drug.

Changing methyl by ethyl at position 9 weakens the contact with Phe330 and strengthens the interaction with Trp84 (see Table 2). Since the methyl group in 9M-HTH lies in a hydrophobic pocket rich in aromatic residues such as Phe288, Phe290, and Phe331, addition of an extra methylene group slightly displaces the drug toward Trp84 without disturbing greatly the interactions with other residues. Inspection of the AChE−drug complex indicates that accommodation of substituents bigger than ethyl at position 9 cannot be easily achieved without altering the binding pocket, which explains the

Table 2. Selected Structural and Energetic Details for the Complexes between the *Torpedo californica* AChE Enzyme and the Hybrid Derivatives

property[a]	9M	3F,9M	9E	3F,9E
rmsD (all)	0.9 (<0.1)	1.3 (<0.1)	1.4 (<0.1)	0.9 (<0.1)
rmsD (subset)	0.7 (<0.1)	1.0 (<0.1)	1.0 (<0.1)	0.7 (<0.1)
d(drug−Trp84)	4.0 (0.5)	4.3 (0.5)	3.8 (0.5)	4.2 (0.5)
α(drug−Trp84)	11.8 (4.7)	15.1 (5.2)	9.1 (4.7)	10.7 (4.7)
d(drug−Phe330)	3.9 (0.5)	3.7 (0.5)	4.6 (0.7)	3.9 (0.5)
α(drug−Phe330)	13.8 (7.0)	9.6 (5.4)	38.5 (14.5)	11.6 (6.9)
d(NH−OC(His440))	2.9 (0.1)	2.9 (0.1)	2.9 (0.1)	2.9 (0.1)
d(NH_2−Od1(Asp72))	5.0 (0.6)	5.2 (0.7)	5.0 (0.6)	4.6 (0.4)
d(NH_2−Od2(Asp72))	6.2 (0.7)	6.3 (0.9)	5.1 (0.7)	5.7 (0.6)
E_{int}(Trp84)	−10.8 (1.3)	−9.8 (1.4)	−12.0 (1.3)	−10.3 (1.2)
E_{int}(Phe330)	−5.4 (0.9)	−6.1 (0.9)	−3.4 (1.1)	−6.1 (1.1)
E_{int}(Asp72)	−47.0 (3.9)	−47.9 (4.5)	−48.5 (3.3)	−51.7 (3.3)
E_{int}(His440)	−17.3 (1.1)	−17.7 (0.9)	−17.3 (1.3)	−17.9 (1.0)
E_{int}(protein+water)	−211.7 (9.8)	−230.0 (12.1)	−235.4 (17.0)	−232.9 (9.2)

[a] rmsD, root-mean-square deviation (Å); *d*, distance (Å); α, angle (deg); E_{int}, interaction energy (kcal/mol) between the drug and residues lying within the cutoff distance. Values averaged for 100 structures collected during the last 0.5 ns of the molecular dynamics simulations. The standard deviation is given in parentheses.

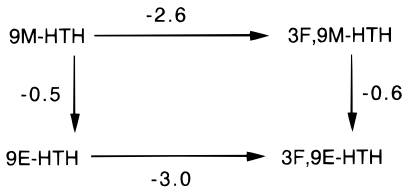

Figure 6. Free energy differences (kcal/mol) for the binding of the 9-methyl (9M), 3-fluoro-9-methyl (3F,9M), 9-ethyl (9E), and 3-fluoro-9-ethyl (3F,9E) derivatives of the tacrine−huperzine A hybrid (HTH) to *Torpedo californica* AChE enzyme.

marked decrease in the inhibitory activity of substituents with propyl, butyl, or phenyl substituents.[11] Attachment of a fluorine atom at position 3 of 9M-HTH or 9E-HTH weakens the interaction with Trp84, while the interaction with Phe330 is improved. The fluorine atom does not establish specific interactions with functional groups of the enzyme, since it fills a hydrophobic pocket formed by Leu333, Met436, Ile439, and Trp432, whose structure is somewhat disrupted compared to the complex between AChE and 9M-HTH. This structural distortion is less important in the 3F,9E-HTH derivative, revealing a mutual compensating effect arising from the need to accommodate the two substituents. Considering the hydrophobic nature of the recognition pocket surrounding position 3, the introduction of apolar groups is expected to be favorable for binding.

The free energy profiles for the mutations in water and in the protein varied smoothly, and no discontinuities were found. Estimates of free energy differences obtained with the first (equilibration) and second (collection) halves of each window were almost identical. Furthermore, the thermodynamic cycles for mutations in water and in the protein (Figure 3, top) were closed with an error lower than 0.3 kcal/mol, which reinforces the reliability of the results.

The predicted differences in binding free energy for mutations converting the 9-methyl substituted hybrid (9M-HTH) into its 3-fluoro (3F,9M-HTH), 9-ethyl (9E-HTH), and 3-fluoro-9-ethyl (3F,9E-HTH) derivatives are given in Figure 6. The results reveal that the effect of the two substitutions examined here are mostly additive, indicating that the 3-fluoro-9-ethyl derivative binds around 3.4 kcal/mol better to the enzyme than the lead compound. This suggests that the active site is flexible enough to accommodate those small structural changes without affecting the drug binding, as expected from the results in Table 2 (see above). Relative to the parent compound, changing the methyl group to ethyl at position 9 has a modest improvement of ∼0.6 kcal/mol, which partly originates from the better desolvation of the ethyl derivative. On the other hand, attachment of a fluorine at position 3 enhances the binding by ∼2.8 kcal/mol. This effect is mainly electrostatic, since the electron-withdrawing character of the fluorine modifies the charge distribution of the quinoline subunit leading to a better interaction with the electrostatic potential created by the cloud of charges in the protein.

Table 3. Relative Free Energy Differences (kcal/mol) Corresponding to the Phe330→Tyr Mutation in the Isolated Enzyme and in the Complexes of AChE with the Four Hybrid Derivatives

isolated AchE	−3.3
9M-HTH	−3.4
3F,9M-HTH	−3.6
9E-HTH	−3.0
3F,9E-HTH	−3.1

It is worth noting that the average interaction energies of the inhibitor with the surrounding (protein + water) environment increases from 9M-HTH to 3F,9M-HTH to 3F,9E-HTH (see Table 2), as expected from the results of TI calculations. The only exception is 9E-HTH, which has the largest interaction energy owing to a very favorable electrostatic contribution. This finding indicates that caution is necessary when binding free energies are predicted using linear response methods, which solely rely on the interaction energy of the inhibitor with its surroundings in the bound and unbound states. These methods are very valuable for a rapid evaluation of binding affinities, but their calibration in a preliminary step is a necessary requisite.

Phe330 → Tyr Mutation. As noted before, TI calculations were performed to explore how the mutation of Phe330 in the *Torpedo californica* enzyme to Tyr, the corresponding residue in human AChE, may influence the binding affinities of the hybrid compounds. This is important since modeling is always done using the structure of the *Torpedo californica* enzyme, while the target of interest is the human enzyme.

Table 3 gives the computed free energy differences for the Phe330→Tyr mutation in the isolated enzyme and in the complexes of AChE with the different

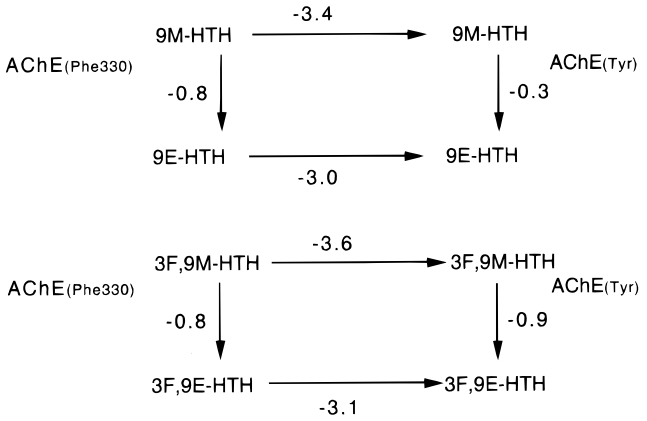

Figure 7. Closure thermodynamic cycles for the mutation of Phe330 to Tyr in the AChE complex with the different inhibitors, and for the mutation of 9M-HTH to 9E-HTH and 3F,9M-HTH to 3F,9F−HTH in the *Torpedo californica* and Phe330 → Tyr mutated AChE. All values are in kcal/mol.

inhibitors (see Figure 3, bottom). In the isolated enzyme such a free energy change amounts to −3.3 kcal/mol, whereas in the AChE−drug complexes the predicted free energy change ranges from −3.0 to −3.6 kcal/mol. Accordingly, the relative binding affinities of the inhibitors for the mutated enzyme are expected to be similar to the values computed for the *Torpedo californica* enzyme. This suggests that the Phe300 → Tyr mutation does not alter remarkably the interaction with the drug, and particularly that the hydroxyl group does not participate directly in drug binding.

To further corroborate this finding, we carried out two sets of additional simulations. First, TI calculations were performed to mutate 9M-HTH to 9E-HTH and 3F,-9M-HTH to 3F,9E-HTH in the AChE enzyme having the Tyr residue. This allows us to form the closure thermodynamic cycles shown in Figure 7 (right vertical arrows), which also shows the free energy changes for mutating Phe330 → Tyr in the AChE−drug complexes (horizontal arrows; see Table 3) and for the mutations 9M-HTH → 9E-HTH and 3F,9M-HTH → 3F,9E-HTH in the *Torpedo californica* enzyme (left vertical arrows). The thermodynamic cycles are closed with an error lower than 0.6 kcal, which gives confidence in the predicted free energy changes. Second, a series of 1 ns MD simulations were conducted for the isolated Phe330→Tyr enzyme and for its complexes with the inhibitors. The analysis of the structures collected in the last 0.5 ns confirms that the hydroxyl group has no direct interaction with the drug, it being solvated on average by one water molecule lying at around 3 Å along all the simulation, as is also observed in the free enzyme.

It is also worthwhile to compare the structural and energetics features of the AChE−drug complexes for the mutated enzyme (Table 4) with the results discussed previously for the *Torpedo californica* one (Table 1). Such a comparison shows a very close similarity in the pattern of interactions irrespective of the inhibitor and of the enzyme, which gives support to the putative binding mode for the hybrid derivatives. The only remarkable difference concerns the 9E-HTH inhibitor, since the ordering of interaction energies between the drug and the surrounding (protein + water) environment now reflects properly the changes in relative binding affinities.

Comparison with Experimental Data. Even though calculations have been performed for the *Torpedo californica* enzyme and the AChE inhibitory assays were performed from bovine erythrocytes,[11] the results reported in the preceding section allow us to compare with some confidence the predicted differences in binding affinity with the experimental changes in inhibitory activity measured for the (−)-enantiomer of these compounds.

Since the substrate concentration in the in vitro assays (performed at 298 K) was the same for all the inhibitors, the experimental differences in binding free energy can be derived from the competitive inhibition equation $IC_{50} = K_i (1 + [S]/K_m)$, where K_m and K_i are Michaelis and enzyme−inhibitor dissociation constants, respectively.[31] The values determined for the changes 9M-HTH → 3F,9M-HTH and 9M-HTH → 9E-HTH are −1.5 and −0.3 kcal/mol, respectively, which compare reasonably well with the predicted estimates of −2.6 and −0.5 kcal/mol (see Figure 6). Our estimate of the good binding of 9M-HTH → 3F,9E-HTH, and the expected good ability of position 3 to accept apolar groups, needs experimental verification, and might encourage further work in the field. Overall, the good quantitative and qualitative agreement found between theoretical calcu-

Table 4. Selected Structural and Energetic Details for the Complexes between the Phe330→Tyr AChE Mutant and the Hybrid Derivatives

property[a]	9M	3F,9M	9E	3F,9E
rmsD (all)	1.0 (<0.1)	1.3 (<0.1)	1.1 (<0.1)	0.9 (<0.1)
rmsD (subset)	0.7 (<0.1)	1.0 (<0.1)	0.9 (<0.1)	0.7 (<0.1)
d(drug−Trp84)	4.1 (0.5)	4.2 (0.5)	3.7 (0.4)	4.0 (0.5)
α(drug−Trp84)	12.5 (5.1)	15.0 (5.3)	12.6 (4.9)	10.2 (5.1)
d(drug−Tyr330)	3.9 (0.5)	3.7 (0.5)	4.6 (0.5)	4.0 (0.5)
α(drug−Tyr330)	13.2 (7.5)	10.0 (6.2)	34.2 (11.8)	13.1 (6.4)
d(NH−OC(His440))	2.9 (0.1)	2.9 (0.1)	2.8 (0.1)	2.9 (0.1)
d(NH_2−Od1(Asp72))	4.8 (0.4)	5.3 (1.0)	6.9 (0.4)	4.7 (0.3)
d(NH_2−Od2(Asp72))	5.9 (0.5)	5.7 (0.6)	5.6 (0.4)	5.6 (0.4)
d(NH_2−OH(Tyr330))	3.4 (0.3)	3.5 (0.3)	3.6 (0.4)	3.5 (0.3)
E_{int}(Trp84)	−10.2 (1.1)	−9.7 (1.4)	−10.8 (1.2)	−10.0 (1.2)
E_{int}(Tyr330)	−6.0 (1.4)	−6.8 (1.4)	−3.8 (1.7)	−7.0 (1.4)
E_{int}(Asp72)	−48.5 (2.8)	−49.5 (4.2)	−39.4 (2.4)	−51.6 (2.7)
E_{int}(His440)	−17.5 (1.0)	−17.5 (1.0)	−17.4 (1.4)	−17.9 (1.2)
E_{int}(protein+water)	−214.6 (10.7)	−231.4 (12.4)	−220.5 (12.8)	−233.6 (10.0)

[a] rmsD, root-mean-square deviation (Å); *d*, distance (Å); α, angle (deg); E_{int}, interaction energy (kcal/mol) between the drug and residues lying within the cutoff distance. Values averaged for 100 structures collected during the last 0.5 ns of the molecular dynamics simulations. The standard deviation is given in parentheses.

lations and experimental data reinforces our confidence in the proposed binding mode as a model to explain the interaction of the tacrine−huperzine A hybrids with the AChE enzyme. Finally, the good performance of the calculations clearly supports the suitability of theoretical approaches such as that used here for the development of new more active anti-Alzheimer drugs targeting AChE.

Conclusion

The whole of the results reported in the preceding sections confirms the suitability of the proposed binding mode of the tacrine−huperzine A hybrids to AChE. The complex between the catalytically active form of the enzyme with the inhibitors shows no relevant structural fluctuations, and the pattern of interactions between drug and enzyme is fully maintained along the simulation. Indeed, this pattern remains essentially unaltered for the different AChE−inhibitor complexes investigated here. The model is able to predict relative binding affinities between the inhibitors that reproduce reasonably well the experimentally measured changes in inhibitory activity. Even though calculations were performed for the *Torpedo californica* enzyme and the inhibitory assays were determined from bovine erythrocytes, the results estimated for the influence of the Phe330−Tyr mutation, which is the most relevant change concerning the binding pocket between the *Torpedo californica* and human enzymes, indicate that this change is expected to have little effect on the predicted binding affinities. Overall, the whole of the results supports the validity of the putative binding model proposed to explain the binding of the tacrine−huperzine A hybrids to AChE. This model will provide a very valuable basis to pursue our current efforts in developing AChE inhibitors with improved inhibitory activity.

Acknowledgment. X.B. thanks the Ministerio de Educación y Ciencia for a fellowship. We thank Prof. P. Camps and Dr. D. Muñoz-Torrero for very helpful discussions. We acknowledge the Fundació La Maratό-TV3 (Project 3004/97) and the Dirección General de Investigación Científica y Técnica (DGICYT; Grant PB97-0908 and PB98-1222) for financial support. We also thank the Centre de Supercomputació de Catalunya (CESCA) for computational facilities.

References

(1) Selkoe, D. J. Normal and Abnormal Biology of the β-Amyloid Precursor Protein. *J. Annu. Rev. Neurosci.* **1994**, *17*, 489−517.

(2) For review, see: Benzi, G.; Moretti, A. Is There a Rationale for the Use of Acetylcholinesterase Inhibitors in the Therapy of Alzheimer's Disease? *Eur. J. Pharmacol.* **1998**, *346*, 1−13.

(3) Tacrine. *Drugs Future* **1987**, *12*, 1032.

(4) Brufani, M.; Filocamo, L.; Lappa, S.; Maggi, A. New Acetylcholinesterase Inhibitors. *Drugs Future* **1997**, *22*, 397−410.

(5) (a) Shutske, G. M.; Pierrat, F. A.; Kapples, K. J.; Cornfeldt, M. L.; Szewczak, M. R.; Huger, F. P.; Bores, G. M.; Haroutunian, V.; Davis, K. L. 9-Amino-1,2,3,4-tetrahydroacridin-1-ols: Synthesis and Evaluation as Potential Alzheimer's Disease Therapeutics *J. Med. Chem*. **1989**, *32*, 1805−1813. (b) Gregor, V. E.; Emmerling, M. R.; Lee, C.; Moore, C. J. The Synthesis and in Vitro Acetylcholinesterase and Butyrylcholinesterase Inhibitory Activity of Tacrine (Cognex) Derivatives. *Bioorg. Med. Chem. Lett.* **1992**, *2*, 861−864. (c) Shutske, G. M.; Bores, G. M.; Bradshaw, K. C.; Huger, F. P.; Kapples, K. J.; Larsen, R. D.; Rush, D. K.; Tomer, J. D. *Bioorg. Med. Chem. Lett.* **1992**, *2*, 865−870. (d) Pang, Y. P.; Quiram, P.; Jelacic, T.; Hong, F.; Brimijoin, S. Highly Potent, Selective, and Low Cost Bis-Tetrahydroaminacrine Inhibitors of Acetylcholinesterase. *J. Biol. Chem.* **1996**, *271*, 23646−23649. (e) Jaen, J. C.; Gregor, V. E.; Lee, C.; Davis, R.; Emmerling, M. Acetylcholinesterase Inhibition by Fused Dihydroquinazoline Compounds. *Bioorg. Med. Chem. Lett.* **1996**, *6*, 737−742.

(6) (a) Brufani, M.; Maurizio, M.; Pomponi, M. Anticholinesterase Activity of a New Carbamate, Hepthylphysostigmine, in View of Its Use in Patients with Alzheimer-type Dementia. *Eur. J. Biochem*. **1986**, *157*, 115−120. (b) Atack, J. R.; Yu, Q. S.; Soncrant, T. T.; Brossi, A.; Rapoport, S. Comparative Inhibitory Effects of Various Physostigmine Analogs Against Acetyl- and Butyrilcholinesterase. *J. Pharmacol. Exp. Ther.* **1998**, *249*, 194−202. (c) Chen, Y. L.; Nielsen, J.; Medberg, K.; Dunaiskis, A.; Jones, S.; Russo, L.; Johnson, J.; Ives, J.; Liston, D. Synthesis, Resolution, and Structure−Activity Relationship of Potent Acetylcholinesterase Inhibitors: 8-Carbaphysostigmine Analogues. *J. Med. Chem*. **1992**, *35*, 1429−1434.

(7) (a) Sumimoto, H.; Iimura, Y.; Yamanishi, Y.; Yamatsu, K. *Bioorg. Med. Chem. Lett.* **1992**, *2*, 871−877. (b) Villalobos, A.; Butler, T. W.; Chapin, D. S.; Chen, Y. L.; DeMattos, S. B.; Ives, J. L.; Jones, S. B.; Liston, D. R.; Nagel, A. A.; Nason, D. M.; Nielsen, J. A.; Ramírez, A. D.; Shalaby, I. A.; White, W. F. 5,7-Dihydro-3-[2-[1-(phenylmethyl)-4-piperidinyl]ethyl]-6*H*-pyrrolo[3,2-f]-1,2-benzisoxazol-6-one: A Potent and Centrally-Selective Inhibitor of Acetylcholinesterase with an Improved Margin of Safety. *J. Med. Chem*. **1995**, *38*, 2802−2808.

(8) Rampa, A.; Bisi, A.; Valenti, P.; Recanatini, M.; Cavalli, A.; Andrisano, V.; Cavrini, V.; Fin, L.; Buriani, A.; Giusti, P. Acetylcholinesterase Inhibitors: Synthesis and Structure−Activity Relationships of omega-(*N*-methyl-*N*-(3-alkylcarbamoyloxyphenyl)-methyl)aminoalkoxy-heteroaryl Derivatives. *J. Med. Chem*. **1998**, *41*, 3976−3986.

(9) (a) Kozikowski, A. P.; Xia, Y.; Reddy, E. R.; Tückmantel, W.; Hanin, I.; Tang, X. C. Synthesis of Huperzine A and its Analogues and their Anticholinesterase Activity. *J. Org. Chem*. **1991**, *56*, 4636−4645. (b) Kozikowski, A. P.; Campini, G.; Sun, L.-Q.; Wang, S.; Saxena, A.; Doctor, B. P. Identification of a More Potent Analogue of the Naturally Ocurring Alkaloid Huperzine A. Predictive Molecular Modeling of its Interaction with AChE. *J. Am. Chem. Soc.* **1996**, *118*, 11357−11362. (c) Kozikowski, A. P.; Campiani, G.; Nacci, V.; Sega, A.; Saxena, A.; Doctor, B. P. An Approach to Modified Heterocyclic Analogues of Huperzine A and Isohuperzine A. Synthesis of the Pyrimidone and Pyrazole Analogues, and Their Anticholinesterase Activity. *J. Chem. Soc., Perkin Trans.* **1996**, 1, 1287−1297. (d) Kozikowski, A. P.; Ding, Q.; Saxena, A.; Doctor, B. P. Synthesis of (±)-10, 10-Dimethyl-Huperzine A−A Huperzine Analogue Possessing a Slower Enzyme Off-Rate. *Bioorg. Med. Chem. Lett.* **1996**, *6*, 259−262. (e) Kaneko, S.; Nakajima, N.; Shikano, M.; Katoh, T.; Terashima, S. Synthetic Studies of Huperzine A and its Fluorinated Analogues. 2. Synthesis and Acetylcholinesterase Inhibitory Activity of Novel Fluorinated Huperzine A Analogues. *Tetrahedron* **1998**, *54*, 5485−5506.

(10) (a) Badia, A.; Baños, J. E.; Camps, P.; Contreras, J.; Görbig, D. M.; Muñoz-Torrero, D.; Simon, M.; Vivas, N. M. Synthesis and Evaluation of Tacrine−Huperzine A Hybrids as Acetylcholinesterase Inhibitors of Potential Interest for the Treatment of Alzheimer's Disease. *Bioorg. Med. Chem*. **1998**, *6*, 427−440. (b) Camps, P.; Contreras, P.; Font-Badia, M.; Morral, J.; Muñoz-Torrero, D.; Solans, X. Enantioselective Synthesis of Tacrine−Huperzine A Hybrids. Preparative Chiral MPLC Separation of their Racemic Mixtures and Absolute Configuration Assignments by X-ray Diffraction Analysis. *Tetrahedron: Asymmetry* **1998**, *9*, 835−849.

(11) Camps, P.; El Achab, R.; Görbig, D. M.; Morral, J.; Muñoz-Torrero, D.; Badia, A.; Baños, J. E.; Vivas, N. M.; Barril, X.; Orozco, M.; Luque, F. J. Synthesis, in vitro Pharmacology and Molecular Modeling of Very Potent Tacrine−Huperzine A Hybrids as Acetylcholinesterase Inhibitors of Potential Interest for the Treatment of Alzheimer's Disase. *J. Med. Chem*. **1999**, *42*, 3227−3242.

(12) Sussman, J. L.; Harel, M.; Frolow, F.; Oefner, C.; Goldman, A.; Toker, L.; Silman, I. Atomic Structure of Acetylcholinesterase from *Torpedo californica*: A Prototypic Acetylcholine-Binding Protein. *Science* **1991**, *253*, 872−879.

(13) Harel, M.; Schalk, I.; Ehret-Sabatier, L.; Bouet, F.; Goeldner, M.; Hirth, C.; Axelsen, P. H.; Silman, I.; Sussman, J. L. Quaternary Ligand Binding to Aromatic Residues in the Active-Site Gorge of Acetylcholinesterase. *Proc. Natl. Acad. Sci. U.S.A.* **1993**, *90*, 9031−9035.

(14) Raves, M. L.; Harel, M.; Pang, Y.-P.; Silman, I.; Kozikowski, A. P.; Sussman, J. L. Structure of Acetylcholinesterase Complexed with the Nootropic Alkaloid, (−)-Huperzine A. *Nature Struct. Biol.* **1997**, *4*, 57−63.

(15) Entries 1ACJ and 1VOT in the Protein Data Bank for the complexes of AChE with tacrine and (−)-huperzine A, respectively, were utilized in molecular modeling studies.

(16) Berstein, F. C.; Koetzle, T. F.; Williams, G. J. B.; Meyer Jr., E. F.; Brice, M. D.; Rodgers, J. R.; Kennard, O.; Shimanouchi, T.; Tasumi, M. The Protein Data Bank: A Computer-Based Archival File for Macromolecular Structures *J. Mol. Biol.* **1977**, *112*, 535−542.
(17) *Insight-II*; Biosym Technologies: San Diego, 1993.
(18) Wlodek, S. T.; Antosiewicz, J.; McCammon, J. A.; Straatsma, T. P.; Gilson, M. K.; Briggs, M. J.; Humblet, C.; Sussman, J. L. Binding of Tacrine and 6-Chlorotacrine by Acetylcholinesterase. *Biopolymers* **1996**, *38*, 109−117.
(19) Hariharan, P. C.; Pople, J. A. *Theor. Chim. Acta* **1973**, *28*, 213−219.
(20) Frisch, M. J.; Trucks, G. W.; Schlegel, H. B.; Gill, P. M. W.; Johnson, B. G.; Robb, M. A.; Cheeseman, J. R.; Keith, T. A.; Petersson, G. A.; Montgomery, J. A.; Raghavachari, K.; Al-Laham, M. A.; Zakrzewski, V. G.; Ortiz, J. V.; Foresman, J. B.; Cioslowski, J.; Stefanov, B. B.; Nanayakkara, A.; Challacombe, M.; Peng, C. Y.; Ayala, P. Y.; Chen, W.; Wong, M. W.; Andres, J. L.; Replogle, E. S.; Gomperts, R.; Martin, R. L.; Fox, D. J.; Binkley, J. S.; Defrees, D. J.; Baker, J.; Stewart, J. P.; Head-Gordon, M.; Gonzalez, C.; Pople, J. A. *Gaussian 94*, Rev. A.1; Gaussian Inc.: Pittsburgh, 1995.
(21) Foye, W. O.; Lemke, T. L.; Williams, D. A. *Principles of Medicinal Chemistry*, 4th ed.; Williams and Wilkins: Media, PA, 1995. Appendix: Table A-1.
(22) Jorgensen, W. L.; Chandrasekhar, J.; Madura, J. D.; Impey, R. W.; Klein, M. L. Comparison of Simple Potential Functions for Simulating Liquid Water. *J. Chem. Phys.* **1983**, *79*, 926−935.
(23) Cornell, W. D.; Cieplak, P.; Bayly, C. I.; Gould, I. R.; Merz, K.; Ferguson, D. M.; Spellmeyer, D. C.; Fox, T.; Caldwell, J. W.; Kollman, P. A Second Generation Force Field for the Simulation of Proteins, Nucleic Acids, and Organic Molecules. *J. Am. Chem. Soc.* **1995**, *117*, 5179−5197.
(24) Bayly, C. I.; Cieplak, P.; Cornell, W. D.; Kollman, P. A. A Well-Behaved Electrostatic Potential Based Method Using Charge Restraints for Deriving Atomic Charges. *J. Phys. Chem.* **1993**, *97*, 10269−10280.
(25) Ryckaert, J. P.; Ciccotti, G.; Berendsen, H. J. C. Numerical Integration of the Cartesian Equations of Motion of a System with Constraints: Molecular Dynamics of *n*-Alkanes. *J. Comput. Phys.* **1977**, *23*, 327−341.
(26) Case, D. A.; Pearlman, D. A.; Caldwell, J. C.; Cheatham, T. E.; Ross, W. S.; Simmerling, C.; Darden, T.; Merz, K. M.; Stanton, R. V.; Cheng, A.; Vincent, J. J.; Crowley, M.; Ferguson, D. M.; Radmer, R.; Seibel, G. L.; Singh, U. C.; Weiner, P.; Kollman, P. A. *AMBER5*; University of California: San Francisco, 1997.
(27) (a) Bashford, D.; Case, D. A.; Choi, C.; Gippert, G. P. A Computational Study of the Role of Solvation Effects in Reverse Turn Formation in the Tetrapeptides APGD and APGN. *J. Am. Chem. Soc.* **1997**, *119*, 4964−4971. (b) Srinivasan, J.; Cheatham, T. E., III; Cieplak, P.; Kollman, P.; Case, D. A. Continuum Solvent Studies of the Stability of DNA, RNA, and Phosphoramidate-DNA Helices. *J. Am. Chem. Soc.* **1998**, *120*, 9401−9409. (c) Jayaram, B.; Sprous, D.; Young, M. A.; Beveridge, D. L. Free Energy Analysis of the Conformational Preferences of A and B Forms of DNA in Solution. *J. Am. Chem. Soc.* **1998**, *120*, 10629−10633.
(28) Sitkoff, D.; Sharp, K. A.; Honig, B. Accurate Calculation of Hydration Free Energies Using Macroscopic Solvent Models. *J. Phys. Chem.* **1994**, *98*, 1978−1988.
(29) Pearlman, D. A. Determining the Contributions of Constraints in Free Energy Calculations: Development, Characterization, and Recommendations. *J. Chem. Phys.* **1993**, *98*, 8946−8957.
(30) Barril, X.; Aleman, C.; Orozco, M.; Luque, F. J. Salt Bridge Interactions: Stability of the Ionic and Neutral Complexes in the Gas Phase, in Solution, and in Proteins. *Proteins* **1998**, *32*, 67−79.
(31) The IC_{50} values determined experimentally for AChE inhibition from bovine erythocytes are 47.1 ± 6.3, 3.5 ± 0.8, and 27.4 ± 3.1 nM for the (−)-enantiomers of 9M-HTH, 3F,9M-HTH, and 9E-HTH, respectively. Data taken from ref 11.
(32) Abbreviations: Alzheimer disease, AD; acetylcholinesterase, AChE; tacrine, THA; huperzine A, HUP; tacrine−huperzine A hybrid, HTH; molecular dynamics, MD; thermodynamic integration, TI; rmsd, root-mean square-deviation.

JM990371U